SUPPLEMENTAL INFORMATION AND SUPPLEMENTARY FIGURES

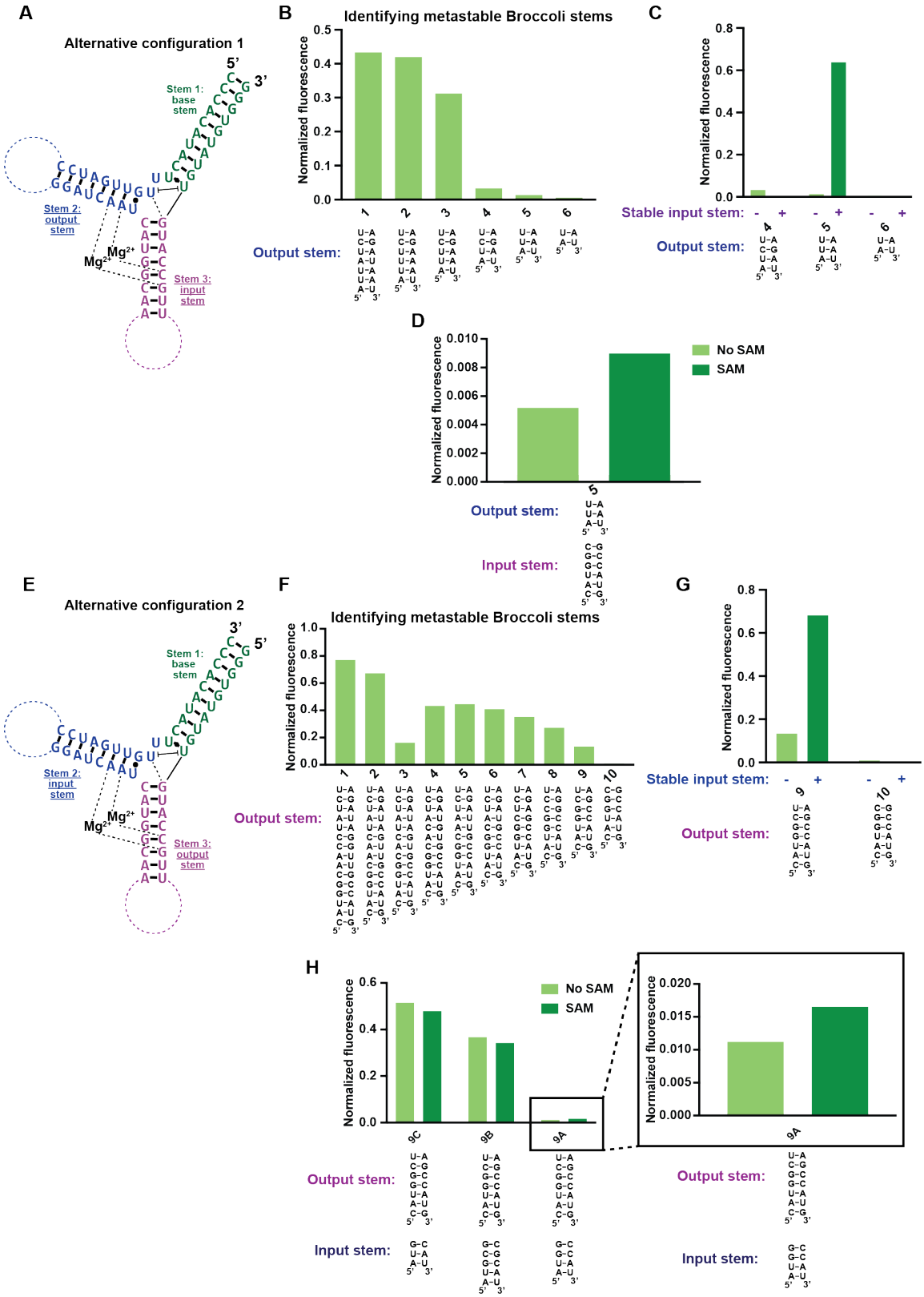

Figure S1. Alternative configurations of F30-based SAM sensors, related to Figures 2 and 3

(**A**) A secondary structure of the Phi29 three-way junction showing Alternative Configuration 1. In this configuration, the stem that was previously the output stem (green) is now the base and contains the 5' and 3' ends. The stem that was previously the input stem (blue) is now the output stem, and Stem 3 (magenta), which was previously the base stem, is now the input stem. Details of the intramolecular interactions are shown in Figure 1.

(**B**) Identifying metastable output stems in Alternative Configuration 1 of the F30 three-way junction. Six different output stem variants were tested. For each sample, the input stem was replaced with a 12-nucleotide, unstructured loop. RNA (0.25 μM) was incubated with 10 μM DFHBI-1T in a buffer containing 140 mM KCl and 1 mM $MgCl_2$. Shown is the fluorescence (Ex 460 nm, Em 505 nm, 1 h, 25°C) normalized to Broccoli fluorescence. Output stem variants 4-6 showed low fluorescence, and were selected for further analysis. Single replicates were performed.

(**C**) Allosteric activation of Broccoli by the input stem in Alternative Configuration 1. Output stem variants 4-6 from (**B**) were assessed for fluorescence recovery when the unstructured loop was replaced with a stable input stem. RNA (0.25 μM) was incubated with 10 μM DFHBI-1T in a buffer containing 140 mM KCl and 1 mM $MgCl_2$. The fluorescence of each sample was measured (Ex 460 nm, Em 505 nm) after incubation at room temperature for 1 h. The fluorescence of each variant is shown in the context of a stable input stem (dark green) normalized to Broccoli fluorescence. Output stem variant 5 showed induction of fluorescence when the unstructured loop in the input stem was changed to a stable stem. Single replicates were performed.

(**D**) SAM-induced Broccoli fluorescence in Alternative Configuration 1. RNA was tested with output stem variant 5 and the SAM aptamer on the input stem. RNA (1 μM) was incubated with 20 μM DFHBI-1T with or without 0.2 mM SAM in a buffer containing 140 mM KCl and 1 mM $MgCl_2$. Shown is the fluorescence (Ex 460 nm, Em 505 nm, 1 h, 25°C) normalized to Broccoli fluorescence. Single replicates were performed.

(**E**) A secondary structure of the Phi29 three-way junction showing Alternative Configuration 2. In this configuration, the previous output stem (green) is now the base and contains the 5' and 3' ends. The previous input stem (blue) is maintained as the input stem, and the previous base stem, i.e., Stem 3 (magenta), is now the output stem. Details of the intramolecular interactions are shown in Figure 1.

(**F**) Identifying metastable output stems in alternative configuration 2 of the F30 three-way junction. Ten different output stem variants were tested. For each sample, the input stem contained a 12-nucleotide, unstructured loop. RNA (0.25 μM) was incubated with 10 μM DFHBI-1T in a buffer containing 140 mM KCl and 1 mM $MgCl_2$. Shown is the fluorescence (Ex 460 nm, Em 505 nm, 1 h, 25°C) normalized to Broccoli fluorescence. Output stem variants 9 and 10 showed low fluorescence, and were selected for further analysis. Single replicates were performed.

(**G**) Allosteric activation of Broccoli by the input stem for Alternative Configuration 2. Output stem variants 9 and 10 of (**F**) were assessed for fluorescence recovery when the unstructured loop on the input stem was replaced with a stable stem. RNA (0.25 μM) was incubated with 10 μM DFHBI-1T in a buffer containing 140 mM KCl and 1 mM $MgCl_2$. The fluorescence of each sample was measured (Ex 460 nm, Em 505 nm) after incubation at room temperature for 1 h. The fluorescence of each variant is shown in the context of a stable input stem (dark green) normalized to Broccoli fluorescence. Output stem variant 9 showed significant induction of fluorescence when the unstructured loop in the input stem (**F**) was changed to a stable stem. Single replicates were performed.

(**H**) SAM-induced Broccoli fluorescence in Alternative Configuration 2. RNA was tested with output stem variant 9 and the SAM aptamer fused to three input stem variants. RNA (1 μM) was incubated with 20 μM DFHBI-1T with or without 0.2 mM SAM in a buffer containing 140 mM KCl and 1 mM $MgCl_2$. Shown is the fluorescence (Ex 460 nm, Em 505 nm, 1 h, 25°C) normalized to Broccoli fluorescence. Single replicates were performed.

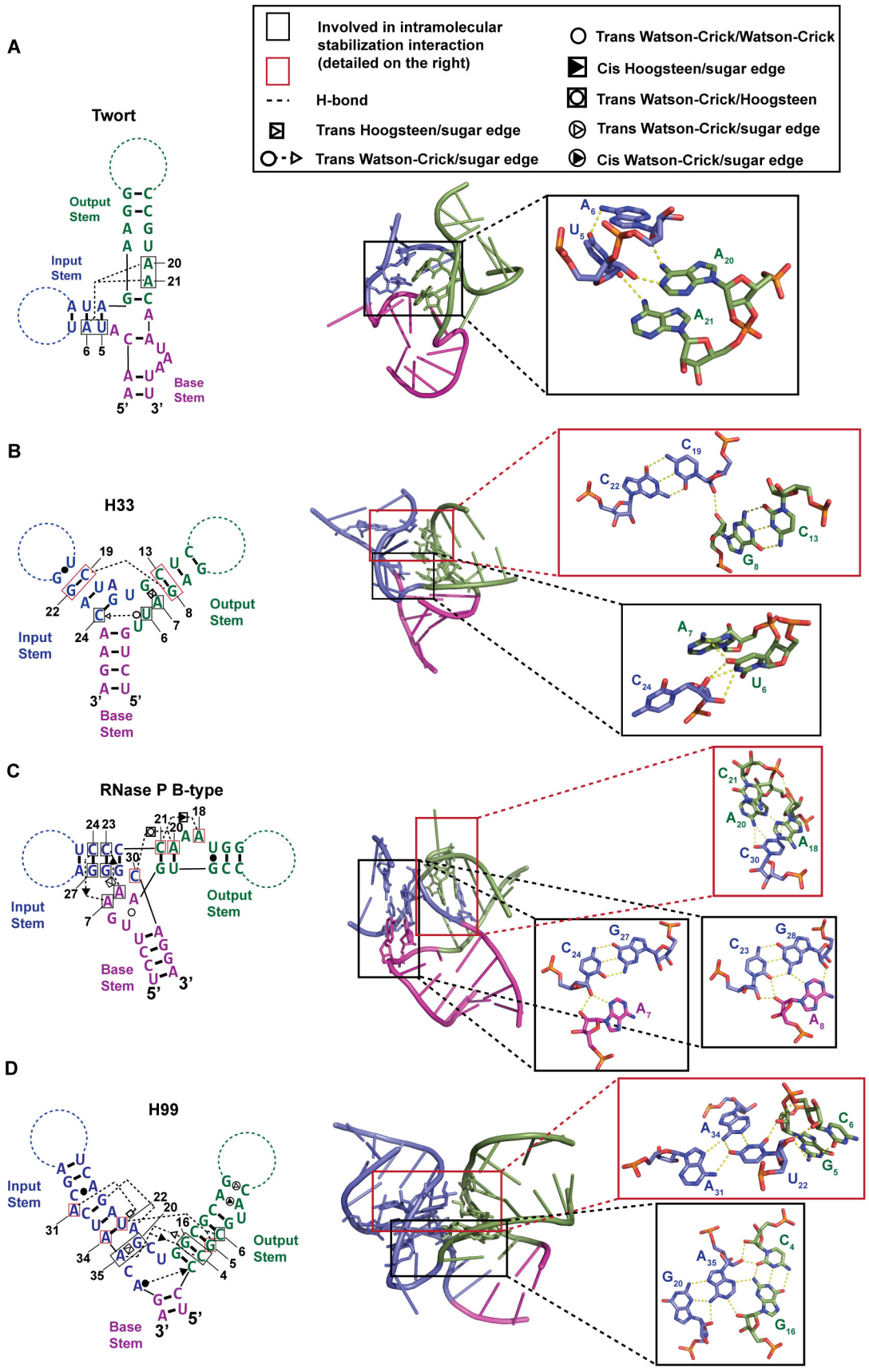
A
Involved in intramolecular stabilization interaction (detailed on the right)
H-bond
Trans Hoogsteen/sugar edge
Trans Watson-Crick/sugar edge
Trans Watson-Crick/Watson-Crick
Cis Hoogsteen/sugar edge
Trans Watson-Crick/Hoogsteen
Trans Watson-Crick/sugar edge
Cis Watson-Crick/sugar edge
Twort
Output Stem
Input Stem
Base Stem
5'
3'
B
H33
Output Stem
Input Stem
Base Stem
C
RNase P B-type
Input Stem
Output Stem
Base Stem
D
H99
Input Stem
Output Stem
Base Stem

Figure S2. Tertiary interactions of different three-way junctions used for sensor design, related to Figure 4

(**A**) (Left) Secondary structure of the Twort three-way junction. The selected output stem (green) and input stem (blue) are indicated. We added six additional base pairs to the selected base stem (magenta). The key at the top defines the symbols used to represent each type of interaction. Tertiary interaction notation is based on Leontis and Westhof (Leontis and Westhof, 2001). Shown are H-bonding interactions formed between output stem nucleotides A20 and A21 (green) and input stem nucleotides U5 and A6 (blue). (Right) Crystal structure of the Twort three-way junction showing the intramolecular interactions described above. The crystal structure of Twort three-way junction shows the overall architecture of the helical stems. The inset shows a detailed view of interactions formed between the Watson-Crick faces of A20 and A21 (green) and the sugar edges of U5 and A6 (blue). The structures shown here are from PDB 1Y0Q (Golden et al., 2005).

(**B**) (Left) Secondary structure of the H33 three-way junction. We added seven additional base pairs to the selected base stem (magenta). Shown is an interaction formed by the Watson-Crick face of U6 (green) of the output stem and the sugar edge of C24 (blue) of the input stem. Also shown is an H-bonding interaction formed by the 2' hydroxyls of G8 (green) and C19 (blue). (Right) The crystal structure shows the overall architecture of helical stems in the H33 three-way junction. The upper inset shows a detailed view of the hydrogen-bonding interaction between the 2'-OH of G8 and the 2'-OH of C19. The lower inset shows a detailed view of the hydrogen-bonding interactions between the Watson-Crick face of U6 and the ribose hydroxyls of C24 The structures shown here are from PDB 1S72 (Klein et al., 2004).

(**C**) (Left) A secondary structure of the RNase P B-type (RNase P) three-way junction. We added six additional base pairs to the selected base stem (magenta). Shown is an interaction formed by the Hoogsteen face of output stem nucleotide C21 (green) and the sugar edge of output stem nucleotide A18 (green). Also shown is an interaction formed by the Watson-Crick face of input stem nucleotide C30 (blue) and the sugar edge of output stem nucleotide A20 (green). The input stem (blue) forms several interactions with the base stem (magenta). The sugar edge of C24 (blue) interacts with the sugar edge of A7 (magenta). The Hoogsteen face of G28 (blue) interacts with the sugar edge of A8 (magenta). The sugar edge of A8 (magenta) also interacts with the sugar edge of C23 (blue). (Right) The crystal structure shows the overall architecture of helical stems in the RNase P three-way junction. The upper inset (red) shows the interactions involving A18, A20, and C21 of the output stem (green) and C30 of the input stem (blue). The left black inset shows interactions between A7 of the base stem (magenta) and C24 or the input stem (blue). The right black inset shows interactions between the input stem base pair G28·C23 (blue) and base stem nucleotide A8 (magenta). The structures shown here are from PDB 1NBS (Krasilnikov et al., 2003).

(**D**) (Left) A secondary structure of the H99 three-way junction. We added eight additional base pairs to the selected base stem (magenta). Shown are several interactions formed between the input stem (blue) and the output stem (green). U22 (blue) forms hydrogen-bonding interactions with G5 and C6 (green). Additionally, the sugar edge of A35 (blue) interacts with sugar edges of C4 and G16 (green). (Right) The crystal structure shows the overall architecture of helical stems in the H99 three-way junction. The red inset shows a detailed view of the hydrogen-bonding network around U22 (blue). The black inset details shows several hydrogen bonds between the sugar edge of A35 (blue) and the sugar edges of C4 and G16 (green). The structures shown here are from PDB 1S72 (Klein et al., 2004).

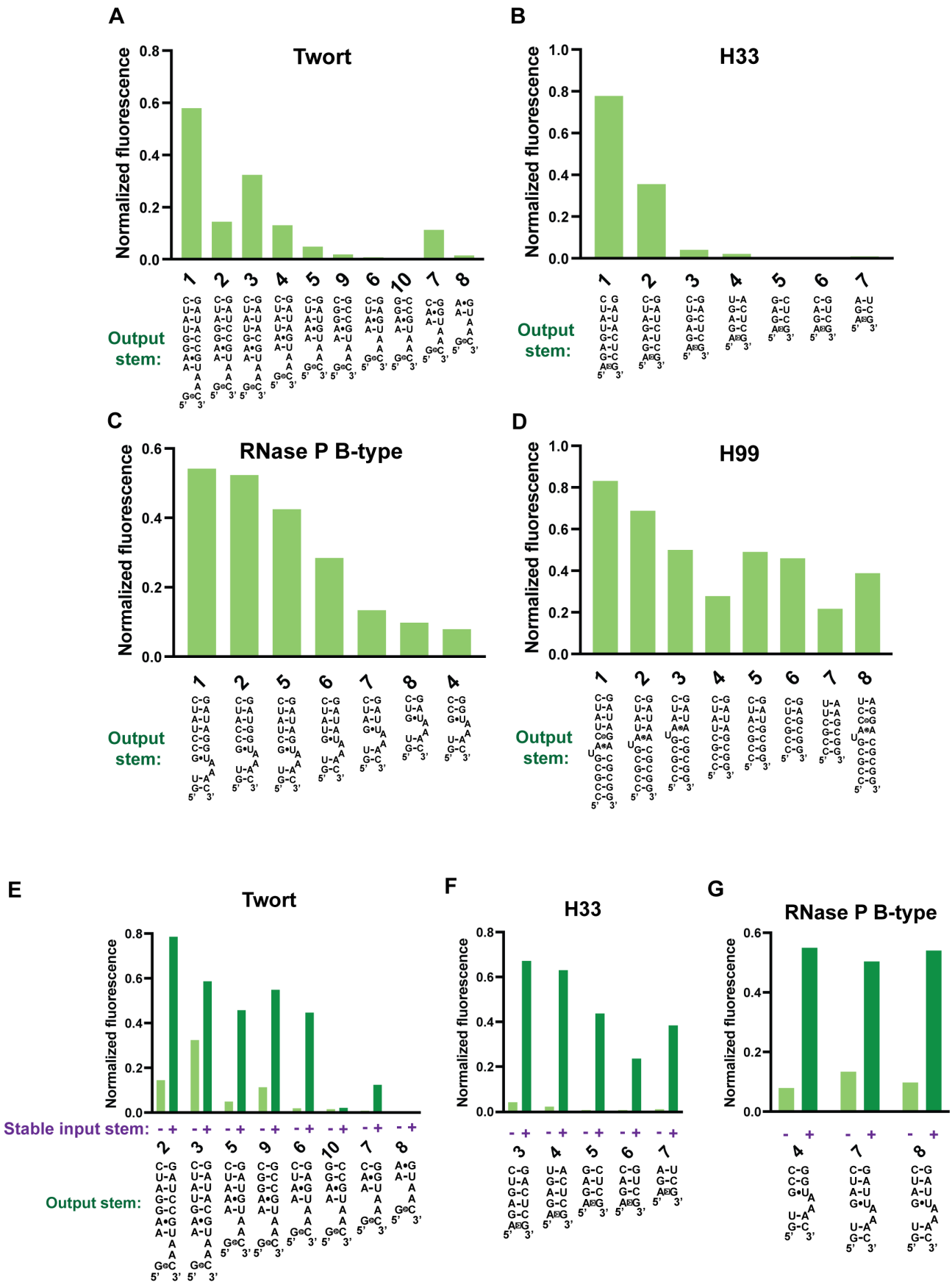
A
Twort
Normalized fluorescence
0.0
0.2
0.4
0.6
0.8
1 2 3 4 5 9 6 10 7 8
Output stem:
B
H33
Normalized fluorescence
0.0
0.2
0.4
0.6
0.8
1.0
1 2 3 4 5 6 7
Output stem:
C
RNase P B-type
Normalized fluorescence
0.0
0.2
0.4
0.6
1 2 5 6 7 8 4
Output stem:
D
H99
Normalized fluorescence
0.0
0.2
0.4
0.6
0.8
1.0
1 2 3 4 5 6 7 8
Output stem:
E
Twort
Normalized fluorescence
0.0
0.2
0.4
0.6
0.8
Stable input stem: - + - + - + - + - + - + - + - +
2 3 5 9 6 10 7 8
Output stem:
F
H33
Normalized fluorescence
0.0
0.2
0.4
0.6
0.8
- + - + - + - + - +
3 4 5 6 7
G
RNase P B-type
Normalized fluorescence
0.0
0.2
0.4
0.6
- + - + - +
4 7 8

Figure S3. Identifying metastable output stems in different three-way junction architectures, related to Figure 4

(**A**) Identifying metastable output stems in the Twort three-way junction. A twelve-nucleotide loop was inserted on the input stem of the Twort three-way junction to prevent any stabilization effect of this stem on the output stem. Ten different output stem variants were tested. In vitro transcribed RNA (0.5 μM) was incubated with 10 μM DFHBI-1T in a buffer containing 140 mM KCl and 1 mM $MgCl_2$. Shown is the fluorescence (Ex 460 nm, Em 505 nm, 1 h, 25°C) normalized to Broccoli fluorescence. Output stem variants 2-10 showed reduced fluorescence and were selected for further analysis. Single replicates were performed.

(**B**) Identifying metastable output stems in the H33 three-way junction. A twelve-nucleotide loop region was inserted on the input stem of the H33 three-way junction to prevent any stabilization effect of this stem on the output stem. Seven different output stem variants were tested using the same conditions as above. Output stem variants 3-7 showed reduced fluorescence and were selected for further analysis. Single replicates were performed.

(**C**) Identifying metastable output stems in the RNase P three-way junction. A twelve-nucleotide loop region was inserted on the input stem of the RNase P three-way junction to prevent any stabilization effect of this stem on the output stem. Seven different output stem variants were tested using the same conditions as above. Output stem variants 4, 7, and 8 showed reduced fluorescence and were selected for further analysis. Single replicates were performed.

(**D**) Identifying metastable output stems in the H99 three-way junction. A twelve-nucleotide loop region was inserted on input stem of the H99 three-way junction to prevent any stabilization effect of this stem on the output stem. Eight different output stem variants were tested using the same conditions as above. Single replicates were performed.

(**E**) Allosteric activation of Broccoli by the input stem in the Twort three-way junction. The loop region on the input stem of the Twort three-way junction was replaced with a stable stem to test the ability of this stem to promote fluorescence activation of Broccoli on the output stem. Eight different output stem variants were assessed for fluorescence activation when the unstructured loop on the input stem (**A**) was replaced with a stable stem. In vitro transcribed RNA (0.5 μM) was incubated with 10 μM DFHBI-1T in a buffer containing 140 mM KCl and 1 mM $MgCl_2$. Shown is the fluorescence (Ex 460 nm, Em 505 nm, 1 h, 25°C) normalized to Broccoli fluorescence. Single replicates were performed.

(**F**) Allosteric activation of Broccoli by the input stem in the H33 three-way junction. The loop region on the input stem of the H33 three-way junction was replaced with a stable stem to test the ability of this stem to promote fluorescence activation of Broccoli on the output stem. Five different output stem variants were assessed for fluorescence activation when the unstructured loop on the input stem (**B**) was replaced with a stable stem. Samples were prepared and tested as (**E**). Single replicates were performed.

(**G**) Allosteric activation of Broccoli by the input stem in the RNase P three-way junction. The loop region on the input stem of the RNase P three-way junction was replaced with a stable stem. Three different output stem variants were assessed for fluorescence activation when the unstructured loop on the input stem (**C**) was replaced with a stable stem. Samples were prepared and tested as (**E**). Single replicates were performed.

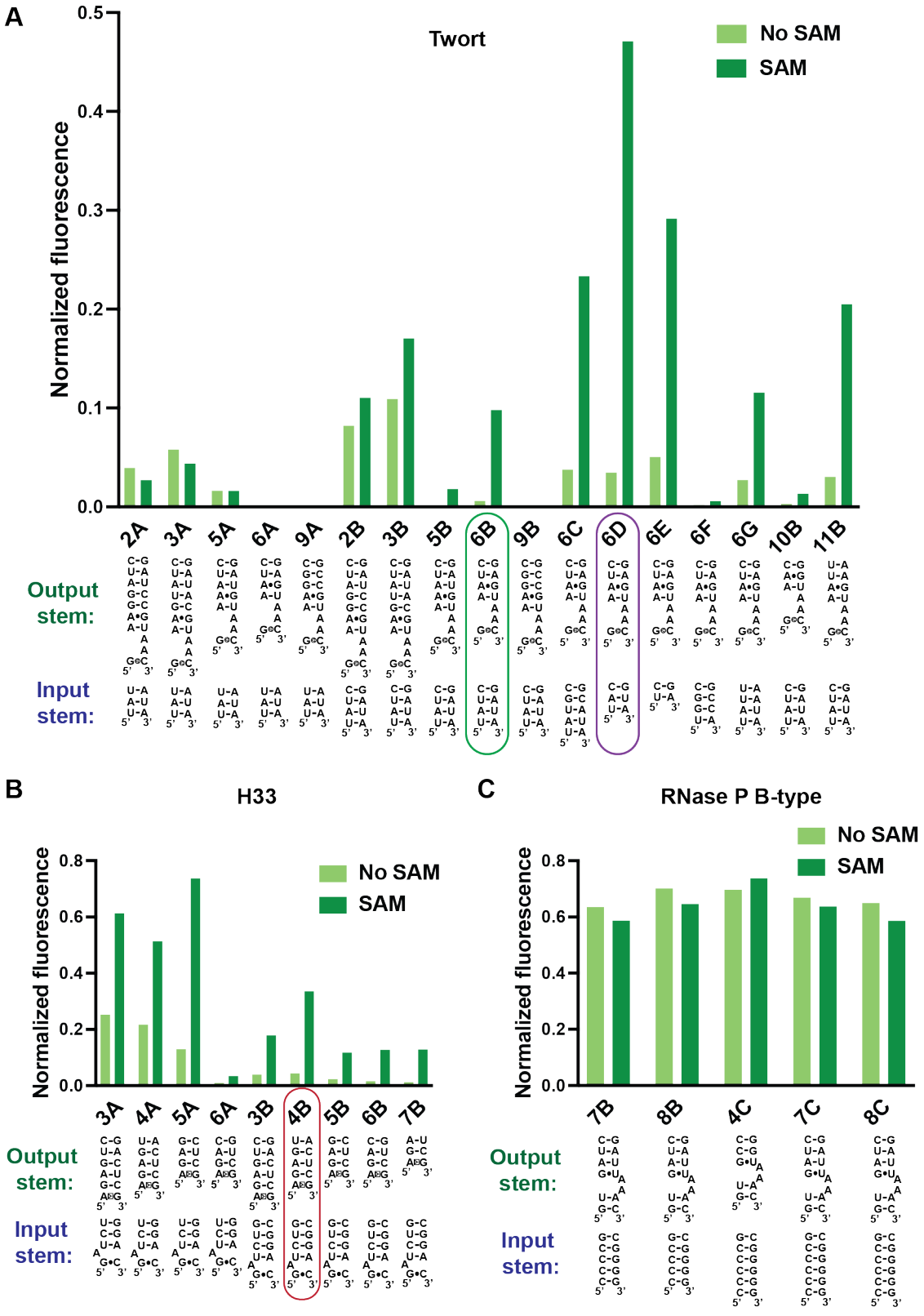
A
Twort
No SAM
SAM
Normalized fluorescence
0.5
0.4
0.3
0.2
0.1
0.0
2A
3A
5A
6A
9A
2B
3B
5B
6B
9B
6C
6D
6E
6F
6G
10B
11B
Output stem:
Input stem:
B
H33
No SAM
SAM
Normalized fluorescence
0.8
0.6
0.4
0.2
0.0
3A
4A
5A
6A
3B
4B
5B
6B
7B
Output stem:
Input stem:
C
RNase P B-type
No SAM
SAM
Normalized fluorescence
0.8
0.6
0.4
0.2
0.0
7B
8B
4C
7C
8C
Output stem:
Input stem:

Figure S4. Optimizing SAM sensors based on the Twort and H33 three-way junctions, related to Figure 4

(**A**) Optimization of input and output stems in Twort-based SAM sensors. Several combinations of input and output stems were tested in Twort-based SAM sensors. 6D and 6B were chosen for further development and renamed Twort A and Twort B, respectively. In vitro transcribed RNA (1 μM) was incubated with 20 μM DFHBI-1T and 1 mM SAM in a buffer containing 140 mM KCl and 1 mM $MgCl_2$. Shown is the fluorescence (Ex 460 nm, Em 505 nm, 1 h, 25°C) normalized to Broccoli fluorescence. Single replicates were performed.

(**B**) Optimization of input and output stems in H33-based SAM sensors. Nine different combinations of input and output stems were tested. In vitro transcribed RNA (0.5 μM) was incubated with 10 μM DFHBI-1T in a buffer containing 140 mM KCl and 1 mM $MgCl_2$. Shown is the fluorescence (Ex 460 nm, Em 505 nm, 1 h, 25°C) normalized to Broccoli fluorescence. H33-4B was chosen for further development. Single replicates were performed.

(**C**) RNase P three-way junction was not optimized into a SAM sensor. Five different combinations of input and output stems were tested. No fluorescence activation was observed in the presence of SAM for any of these RNase P constructs. Samples were prepared and tested as (**A**). Single replicates were performed.

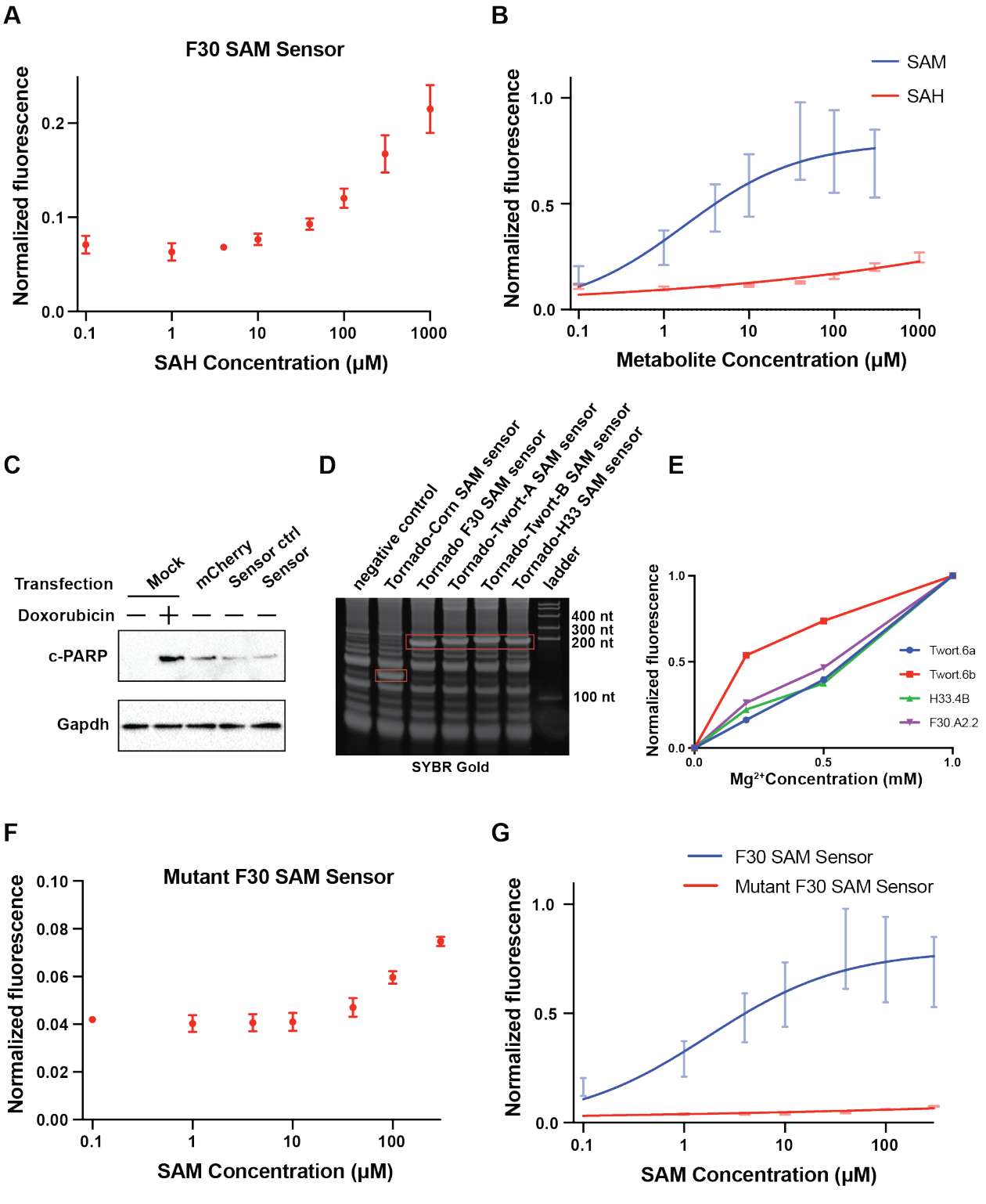
A
F30 SAM Sensor
Normalized fluorescence
SAH Concentration (μM)
B
SAM
SAH
Normalized fluorescence
Metabolite Concentration (μM)
C
Transfection
Mock
mCherry
Sensor ctrl
Sensor
Doxorubicin
c-PARP
Gapdh
D
negative control
Tornado-Corn SAM sensor
Tornado F30 SAM sensor
Tornado-Twort-A SAM sensor
Tornado-Twort-B SAM sensor
Tornado-H33 SAM sensor
ladder
400 nt
300 nt
200 nt
100 nt
SYBR Gold
E
Normalized fluorescence
Twort.6a
Twort.6b
H33.4B
F30.A2.2
Mg2+Concentration (mM)
F
Mutant F30 SAM Sensor
Normalized fluorescence
SAM Concentration (μM)
G
F30 SAM Sensor
Mutant F30 SAM Sensor
Normalized fluorescence
SAM Concentration (μM)

Figure S5. Cytotoxicity, metabolite-binding properties, and expression levels of three-way junction-based SAM sensors, related to Figures 5 and 6.

(**A**) Dose-response curve for fluorescence activation of F30-based SAM sensor by SAH. In vitro transcribed F30-based SAM sensor RNA (50 nM) was incubated with the indicated concentration of SAH in a buffer containing 10 μM DFHBI-1T, 140 mM KCl, and 1 mM $MgCl_2$. Shown is the fluorescence (Ex 460 nm, Em 505 nm, 1 h, 37°C) normalized to Broccoli fluorescence. The mean and SEM are shown (n=3). Note the y-axis in this panel compared to (**B**).

(**B**) Comparison of F30-based SAM sensor dose-response curves by SAH and SAM. In vitro transcribed F30-based SAM sensor RNA (50 nM) was incubated with each indicated concentration of SAM (blue) or SAH (red) in a buffer containing 1 μM DFHBI-1T, 140 mM KCl, and 1 mM $MgCl_2$. SAM titration measurements (blue) also shown in Figure 4C. SAH titration measurements (red) same as (**A**). Curves are results of nonlinear regression of the data fit with specific binding curves. The mean and SEM are shown (n=3).

(**C**) Assessment of apoptosis in cells expressing circular RNA sensors. Western blot of PARP cleavage was used to assay apoptosis in cells transfected with circular F30-based sensor expression plasmids. Total protein was harvested from HeLa cells 48 h after transfection. As a control, total protein was harvested 24 h after treatment with doxorubicin (1 μg/ml). Protein was then separated by PAGE and transferred to membranes. Blots were probed with antibody for cleaved PARP (C-PARP) and GAPDH. The western blot signal is shown. "mCherry" refers to cells transfected with a plasmid that expresses mCherry. "Sensor Control" refers to cells transfected with a plasmid that expresses circular F30-Broccoli RNA, a constitutively fluorescent RNA that is not responsive to SAM. "Sensor" refers to cells transfected with a plasmid that expresses circular F30-based SAM sensor RNA. No increase in PARP cleavage is seen beyond the level seen in cells transfected with the mCherry plasmid.

(**D**) Expression levels of SAM sensor RNA expressed using the Tornado system. To compare expression levels of each circular three-way junction-based SAM sensor, we harvested total cellular RNA from HEK293T cells expressing circular three-way junction-based SAM sensors. 48 h prior to harvesting total RNA, these cells were transfected with circular three-way junction-based SAM sensor plasmid. As a positive control, we harvested total RNA from HEK293T cells expressing circular Corn-based SAM sensor. We harvested total RNA from untransfected HEK293T cells to use as a negative control. RNA (1.5 μg) was loaded in each lane of a 10% TBE-urea polyacrylamide gel. The Riboruler low-range ladder was loaded in lane 7. After polyacrylamide gel electrophoresis, the gel was stained with SYBR Gold to view total RNA. The SYBR Gold stained gel was imaged at the relevant channel (Ex 302 nm; Em 590/110 nm). The red boxes indicate bands corresponding to SAM sensor RNA. Each SAM sensor band is of similar intensity suggesting that differences in expression do not explain differences in cellular fluorescence.

(**E**) Magnesium dependence of three-way junction-based SAM sensors. We titrated in vitro-transcribed three-way junction-based SAM sensors with $MgCl_2$ to determine the EC_{50} of each three-way junction-based SAM sensor for Mg^{2+}. In vitro transcribed RNA (0.5 μM) was incubated with 10 μM DFHBI-1T and 0.1 mM SAM in a buffer containing 40 mM HEPES, 140 mM KCl and the indicated concentration of $MgCl_2$ at pH 7.5. The fluorescence of each sample was measured (Ex 460 nm, Em 505 nm) after incubation at room temperature for 1 h. Data represents single replicates.

(**F**) Dose-response curve for fluorescence activation of Mutant F30-based SAM sensor by SAM. In vitro transcribed Mutant F30-based SAM sensor RNA (50 nM) was incubated with each indicated concentration of SAM in a buffer containing 10 μM DFHBI-1T, 140 mM KCl, and 1 mM $MgCl_2$. Shown is the fluorescence (Ex 460 nm, Em 505 nm, 1 h, 37°C) normalized to Broccoli fluorescence. The mean and SEM are shown (n=3).

(**G**) Comparison of Mutant F30-based SAM sensor and F30-based SAM sensor dose-response curves by SAM. In vitro transcribed Mutant F30-based SAM sensor RNA (50 nM) (red) or F30-based SAM sensor RNA (50 nM) (blue) was incubated with each indicated concentration of SAM in a buffer containing 1 μM DFHBI-1T, 140 mM KCl, and 1 mM $MgCl_2$. F30-based SAM sensor titration measurements (blue) also shown in Figure 4C. Mutant F30 SAM Sensor titration measurements (red) were performed in the same way as (**F**). Curves are results of nonlinear regression of the data fit with specific binding curves. The mean and SEM are shown (n=3).

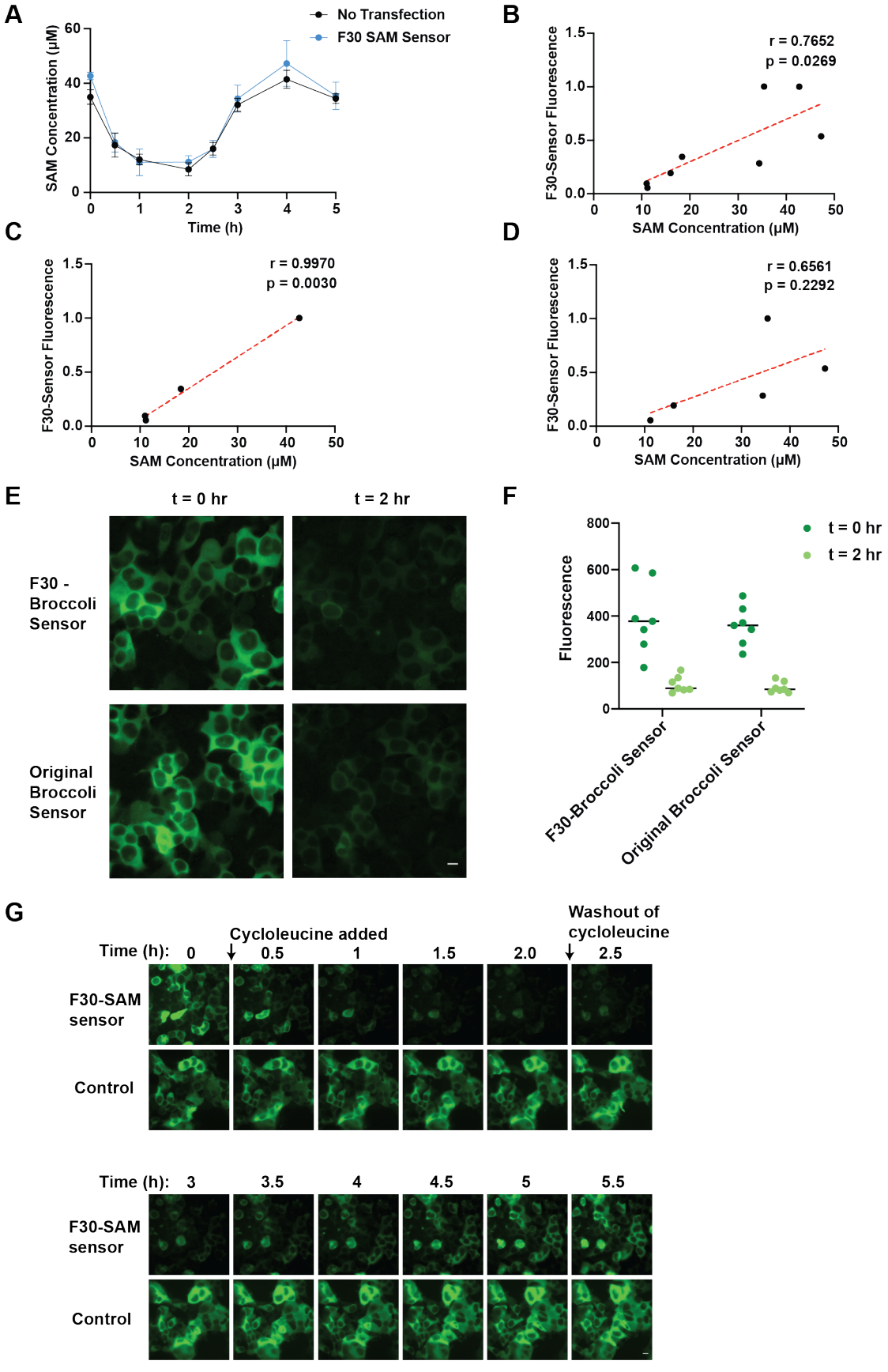
A
No Transfection
F30 SAM Sensor
SAM Concentration (μM)
Time (h)
B
r = 0.7652
p = 0.0269
F30-Sensor Fluorescence
SAM Concentration (μM)
C
r = 0.9970
p = 0.0030
F30-Sensor Fluorescence
SAM Concentration (μM)
D
r = 0.6561
p = 0.2292
F30-Sensor Fluorescence
SAM Concentration (μM)
E
t = 0 hr
t = 2 hr
F30 - Broccoli Sensor
Original Broccoli Sensor
F
t = 0 hr
t = 2 hr
Fluorescence
F30-Broccoli Sensor
Original Broccoli Sensor
G
Time (h): 0
Cycloleucine added
0.5
1
1.5
2.0
Washout of cycloleucine
2.5
F30-SAM sensor
Control
Time (h): 3
3.5
4
4.5
5
5.5
F30-SAM sensor
Control

Figure S6. Additional data from live-cell imaging of SAM dynamics using an F30-based SAM sensor, related to Figure 6

(**A**) SAM levels are reduced after cycloleucine treatment based on a biochemical assay for SAM. Intracellular SAM concentrations were measured using a commercially available assay - Bridge-It® SAM Fluorescence Assay Kit. HEK293T cells expressed in a 6-well plate were either transfected with an F30-based SAM sensor transfection plasmid (F30 SAM Sensor) (blue) or left untransfected (No Transfection) (black). Comparable experimental conditions as used in Figure 6 were initiated approximately 36 h after transfection. At t = 0 h, cycloleucine (50 mM final concentration) was added to cells. At t = 2 h, cellular media was aspirated from the cells, cells were washed with 1xPBS once, and cycloleucine-free media was added to each well. Cell lysates were harvested at each indicated time point and then SAM levels were measured according to the manufacturer's protocol via comparison to a standard curve made using signal from samples of known SAM concentration. As shown, cycloleucine markedly reduces intracellular SAM levels, and SAM levels are restored after cycloleucine is removed. Mean and SEM are shown (n=3).

(**B**) Correlation of SAM concentration to F30-based SAM sensor cellular fluorescence from t = 0 h to t = 5.5 h. Correlation analysis was performed between SAM concentration values from F30-based SAM sensor-expressing cells (**A**) and F30-based SAM sensor average cellular fluorescence (n = 23 cells) (**Figure 6B**) at each indicated time point. Pearson correlation r and two-tailed p-value are shown.

(**C**) Correlation of SAM concentration to F30-based SAM sensor cellular fluorescence from t = 0 h to t = 2 h. Correlation analysis was performed between SAM concentration values from F30-based SAM sensor-expressing cells (n = 23 cells) (**A**) and F30-based SAM sensor average cellular fluorescence values (**Figure 6B**) using only the timepoints from t = 0 h to t = 2 h. Pearson correlation r and two-tailed p-value are shown.

(**D**) Correlation of SAM concentration to F30-based SAM sensor cellular fluorescence from t = 2h to t = 5.5h. Correlation analysis was performed between SAM concentration values for F30-based SAM sensor-expressing cells (**A**) and F30-based SAM sensor average cellular fluorescence values (n = 23 cells) (**Figure 6B**) using only the timepoints from t = 2 h to t = 5.5 h. Pearson correlation r and two-tailed p-value are shown.

(**E**) Representative images comparing F30-based SAM sensor cellular fluorescence to the original Broccoli SAM sensor cellular fluorescence. HEK293T cells were transfected with plasmids expressing the either circular F30-based SAM sensor or the original Broccoli SAM sensor expressed as an RNA circle (Litke and Jaffrey, 2019). Two days after transfection, we imaged cells for 2 h after addition of 25 mM cycloleucine. Cells showed a drop in F30-based SAM sensor fluorescence after cycloleucine treatment. Images were acquired using a 40x objective (NA 0.75) and a FITC filter cube. Acquisition time 500 ms. Scale bar 10 μm.

(**F**) Quantification of cellular fluorescence (n = 7 cells per condition) from F30-based SAM Sensor-expressing cells and Broccoli SAM sensor-expressing cells. Total cellular fluorescence from individual cells expressing the F30-based SAM sensor was calculated from images at t=0h (dark green) and t=2h (light green).

(**G**) Larger fields of view for live-cell SAM imaging. Wider fields of view for single-cell imaging data of circular F30-based SAM sensor fluorescence in response to cycloleucine treatment. Shown are larger fields of view for data from **Figure 6A**. These images allow the changes in cellular fluorescence to be seen in more cells. HEK293T cells were transfected with plasmids expressing the circular F30-based SAM sensor. As a control, we used cells transfected with a plasmid expressing circular F30-Broccoli—the fluorescence of this RNA should not be regulated by intracellular SAM levels. Two days after transfection, we imaged cells for 2 h after addition of 50 mM cycloleucine. We imaged cells for an additional 3.5 h following withdrawal of cycloleucine from the cell culture media. Cells showed a drop in F30-based SAM sensor fluorescence after cycloleucine treatment, and recovery of fluorescence after washing out cycloleucine. Control cell fluorescence stayed consistently high over the course of the experiment. Images were acquired using a 40x objective (NA 0.75) and a FITC filter cube. Acquisition time 500 ms. Scale bar 10 μm.